Single-Cell and Spatial Transcriptomic Analyses Reveals the Dynamic Transcript Profiles of Myocardial Lymphangiogenesis post Myocardial Infarction

Jiaqi He[1,2] †, Dali Zhang[2] †, Haixu Song[2], Ziqi Liu[2], Dan Liu[2], Xiaolin Zhang[2], Xiaojie Zhao[2], Yan Zhang[2], Jing Liu[2], Jiaxin Xu[2], Chenghui Yan[2,*], Yaling Han[1,2,*]

[1]Graduate School, Army Medical University, Chongqing, China

[2]State Key Laboratory of Frigid Zone Cardiovascular Disease, Cardiovascular Research Institute and Department of Cardiology, General Hospital of Northern Theater Command, Shenyang, China

Jiaqi He[1,2] †and Dali Zhang[2] † These authors contributed equally to this work and share first authorship.

*For correspondence:

Yaling Han, MD, PhD

Graduate School, Army Medical University, Chongqing, China; State Key Laboratory of Frigid Zone Cardiovascular Disease, Cardiovascular Research Institute and Department of Cardiology, General Hospital of Northern Theater Command, Shenyang, China. Tel: (0086)–24–28856123, Email: hanyaling@163.net

Chenghui Yan, MD, PhD

State Key Laboratory of Frigid Zone Cardiovascular Disease, Cardiovascular Research Institute and Department of Cardiology, General Hospital of Northern Theater Command, Shenyang, China. Tel: (0086)–24–28856123, Email: yanch1029@163.com

Keywords: Myocardial infarction; Cardiac lymphatics; Single cell sequencing; Spatial transcriptomic; Aquaporin-1; Galectin-9

Abstract

Cardiac lymphatics play an important role in myocardial edema and inflammation. This study integrated single-cell sequencing data and spatial transcriptome data from mouse heart tissue at different time points post-myocardial infarction (MI), and identified four transcriptionally distinct subtypes of lymphatic endothelial cells(LECs) and localized them in space. Interestingly, LECs subgroups was found to be localized in different zones of infarcted heart related to different functions. Additionally, LEC capillary III(LEC ca III) may be involved in the direct regulation of myocardial injuries in infarcted zone from the perspective of metabolic stress, while LEC ca II may be related to the rapid immune inflammatory responses of the border zone in the early stage of MI. LEC ca I, as well as LEC collection mainly participate in the regulation of myocardial tissue edema resolution in the middle and late stages post-MI. Cell trajectory and Cell-Chat analyses further identified that LECs may regulate myocardial edema through Aqp1, and might affect the infiltration of macrophages through the galectin9-CD44 pathway. Collectively, our study revealed the dynamic transcriptional heterogeneity distribution of LECs in different regions of the infarcted heart, in detail; these LECs formed different functional subgroups, that might exhibit different bioeffects in myocardial tissue post-MI.

1 Introduction

The lymphatic vasculature, which accompanies the blood vasculature in most organs, is indispensable for maintaining of tissue fluid homeostasis, immune surveillance and lipid uptake and transport(Alitalo, Tammela, & Petrova, 2005; Huang, Elvington, & Randolph, 2015; Petrova & Koh, 2020). In contrast to circulatory blood vessels, lymphatic vessels are structurally blind-ended segments, that are designed to absorb interstitial fluid and immune cells. These lymphatic capillaries converge onto deeper lymphatic structures called collecting vessels, which are equipped with valves and a muscular wall that promote unidirectional transport and drain extravascular fluid, macromolecules and immune cells(Alitalo, 2011; Oliver, Kipnis, Randolph, & Harvey, 2020).

The cardiac lymphatic vasculature was first described in the 17th century(Tammela & Alitalo, 2010). To date, studies have demonstrated the role of the lymphatic system only in embryonic heart development and cardiac health in adults(Brakenhielm & Alitalo, 2019; Heron, Ratajska, & Brakenhielm, 2022; Klotz et al., 2015). Cardiac lymphatics can take up inter-tissue fluid and transport immune cells through highly branched, blunt, open-ended lymphatic capillaries, to the lymph nodes near the thoracic ducts and, finally, into the superior vena cava(Huang, Lavine, & Randolph, 2017).

Myocardial infarction (MI) is one of the most important cardiovascular diseases. Myocardial edema and inflammation are the two dominant pathological processes in the early stages of MI(Anzai, Ko, & Fukuda, 2022; Bulluck, Dharmakumar, Arai, Berry, & Hausenloy, 2018; Chen, Zhao, & Yan, 2022; Nahrendorf, Pittet, & Swirski, 2010). Many preclinical studies have revealed severe remodeling of lymphatic system during MI in animal models(Ishikawa et al., 2007; Shimizu et al., 2018; Vuorio et al., 2018). The stimulation of cardiac lymphangiogenesis by adrenomedullin or

vascular endothelial growth factor C can ameliorate myocardial edema following MI(Henri et al., 2016; Trincot et al., 2019). However, owing to the extremely low number of lymphatic vessels in the myocardial tissue, there is still a lack of comprehensive and in-depth understanding of the pathological mechanisms underlying myocardial injury and prognostic progression after MI.

With the rapid development of single-cell transcriptome sequencing and spatial single-cell transcriptome sequencing technologies, researchers can explore cell subpopulations, heterogeneity, function, metabolism, and cell-cell interactions at the single-cell level(Grün & van Oudenaarden, 2015; Vandereyken, Sifrim, Thienpont, & Voet, 2023). In order to further elucidate the effects and regulatory mechanisms of the lymphatic vessels in the repair process of myocardial injury following MI. This study, integrated single-cell sequencing and spatial transcriptome data from mouse heart tissue at different time points after MI from publicly available data (E-MTAB-7895, GSE214611) in the ArrayExpress and gene expression omnibus (GEO) databases. By reanalyzing these data, this study revealed dynamic transcriptional heterogeneity and spatial localization differences in regenerated lymphatic endothelial cells (LECs) in heart tissue after MI. Different subpopulations of lymphocytes appear at different times and locations during the process of myocardial post-MI, and perform different biological functions. Furthermore, we validated two key regulatory molecules that play important regulatory roles in myocardial edema and lymphatic immune regulation after MI.

2 Results

2.1 Dynamic Changes of Cardiac Lymphatics in Cardiac Tissue post-MI

To explore the physiological and pathological functions of cardiac lymphatic vessels after myocardial infarction (MI), we established an MI mouse model by ligating the anterior descending branch of the coronary artery (n=32) (Figure1-figure supplement 1A). Heart function was evaluated by micro-ultrasound, and mouse hearts were harvested at 0, 3, 7, 14, and 28 days after MI (n=5-7/ per time-point) (Figure1-figure Supplement 1B). Immunofluorescence (IF) staining was performed using antibodies against Prospero homeobox 1 (PROX1, nuclear protein) and the lymphatic vessel endothelial hyaluronan recetor-1 (LYVE1, membrane protein), both of which specifically labeled the LECs (Figure1- Figure Suppl-1C and 1D). Since the membrane protein LYVE1 can present lymphatic vessel morphology more clearly than PROX1. LYVE1 was used for lymphatic vessel staining at 0, 3, 7, 14, and 28 days after MI (Figure 1A). There were significant differences in the morphology and distribution of the newly formed lymphatic vessels in different regions of the heart tissue post-MI (Figure 1B). Three days post-MI, lymphatic vessels in the infarcted zone (IZ) and border zone (BZ) were significantly lost. However, on the 7th day, a large number of newly formed and dilated continuous lymphatic vessels appeared in the BZ. In the IZ, only a small number of small LYVE1-labeled lymphatic capillaries with discontinuous walls were observed. On the 14th and 28th days following the infarction, the number of lymphatic capillaries in the IZ significantly increased. Continuous large lymphatic collecting vessels were observed in the epicardium of the IZ, and the number of large lymphatic collecting vessels in the BZ did not decrease (Figures. 1A and 1B). In addition, there were no significant changes in the distribution and morphology of cardiac lymphatic vessels in the unaffected normal myocardial area (remote zone, RZ) at any time (Figure1-

figure Supplement 1E and 1F). These results suggest that lymphatic regeneration may be involved in the regulation of myocardial damage following MI.

2.2 Identification of Four Transcriptionally Distinct Subtypes of Regenerated Lymphatic Endothelial Cells in Myocardial Tissue post-MI via Single-Cell Sequence.

To further clarify why the regenerated cardiac LECs mapped to a particular distribution during cardiac repair post-MI, a set of published single-cell sequencing data (E-MTAB-7895) was selected from the ArrayExpress database of mouse MI models at different time points (days 0, 1, 3, 7, 14 and 28). Using specific marker proteins as cell-clustering markers, the cluster dimensionality reduction analysis of the 10,519 single cells (excluding myocardial cells) in this experimental dataset was recalculated. First, we classified these cells into five categories based on specific genes: endothelial cells (Cdh5, Pecam1, and Vwf), fibroblasts (Dcn, Col1a1, and Gsn), immune cells (Ptprc, and C1qa), myocardial fibroblasts (Cthrc1, and postn), smooth muscle cells and pericytes (Myh11, Tagln, Acta2, Rgs5, Abcc9, and Kcnj8) (Figures. 2A and 2B). Subsequently, the endothelial cells (Cdh5, Pecam1, and Vwf) were further clustered into five sub-clusters, including angiogenic endothelial cells (Col4a2, Apln, Sparcl1, and Aplnr), arterial endothelial cells (Fbln5, Hey1, Sema3g, and Efnb2), capillary endothelial cells (Kdr, Rgcc, Aqp1, and Endou), venous endothelial cells (Mgp, Cfh, Bgn, Vwf, and Plvap), and LECs (Lyve1, Cldn5, and Prox1) (Figures. 2C and 2D). To further characterize LECs, we examined the expression of Foxp2, Ackr4, Cavolin-1(Cav1), Nt5e, Pdpn and Lyve1(Takeda et al., 2019). Consistent with this report, the collecting lymphocyte marker Cav1 was expressed in the clusters LEC collecting (LEC co), LEC capillary I (LEC ca I), and LEC capillary III (LEC ca III) clusters, whereas Foxp2 and Ackr4 were expressed almost exclusively in LEC co clusters. Capillary markers Pdpn and Lyve1 were expressed in four subsets, but showed the highest expression in LEC ca III, and the lowest in LEC co (Figures. 2E and 2F). Together, these results indicate significant transcriptional heterogeneity in the regenerated cardiac LECs post-MI.

2.3 Relationship Between the Spatial Localization and Function of LEC Subpopulations post-MI

To elucidate the biological functions of LECs subgroups in myocardial tissue post-MI, we first observed dynamic changes in the number and proportion of LECs subsets after MI. Consistent with the results of IF staining, the number of LECs was significantly reduced in the early phases of MI (D1 and D3). From D7, the number of cells gradually increased and returned to normal levels within 14 days. The regeneration ratios of the four myocardial tissue subsets were significantly different. Normal myocardial tissues are mainly composed of LEC ca I, LEC ca II, and LEC co, with a small amount of LEC ca III. In the early stages of myocardial infarction (D1 and D3), although the number of LECs sharply decreased, the proportion of LEC ca III significantly increased. By D7, there was a significant decrease in LEC ca III with a gradual increase in LEC ca II and LEC co. From D14, the proportion of LEC ca I region significantly increased. Twenty-eight days post-MI, the number and proportion of the three capillary LECs had returned to normal, except for a small proportion of LEC co in the group (Figures. 3A and 3B).

To validate whether these LEC subpopulations are involved in the repair of myocardial injury following MI, we retrieved published single-cell nuclear transcriptomic and spatial transcriptomic data (GSE214611) of mouse MI models from the GEO database. In early MI (D3), LEC ca I, ca III and LEC co were mainly distributed in the IZ and BZ, with LEC ca III being significantly higher in the IZ. In contrast, LEC ca II was mainly distributed in the BZ and RZ, and was significantly reduced in the IZ. As the morphology of the infarcted area gradually became clear, on D7, LEC ca I continued to increase in the IZ region, LEC ca III was still mainly distributed in the IZ, LEC co migrated from the BZ to the IZ, and LEC ca II showed no significant spatial localization or expression differences, but were still highly expressed in the BZ and RZ (Figure 3C).

KEGG functional enrichment analysis was conducted on the genes of the four LEC subtypes. LEC ca III, the LEC subgroup with the highest proportion expressed in the IZ during the early stage of MI, was found to primarily participate in energy metabolism such as oxidative phosphorylation, thermogenesis, glycolysis/gluconeogenesis, antigen presentation, cell morphology and migration related functions. Although ca I and ca III have similar spatial localization after MI, their expression levels were lower than that of LEC ca III on D3, but significantly increased in the IZ on D7. LEC ca I was found primarily participate in the activation of infection, apoptosis, mitophagy, and water absorption related regulation of vasopressin. LEC co showed partial similarity in biological functions with ca I, and were mainly involved in fluid regulation and flow, such as renin, saliva secretion, and inflammation. LECs are inconsistently is involved in the regulation of RNA transport, degradation, and ferroptosis. LEC ca II, which significantly reduced in IZ, while sustaining high expression in the BZ and RZ, is mainly related to NFκB is associated with the regulation of chemokine signaling pathways and cytokine interactions between ligands (Figure 3E).

In summary, based on the pathological changes in myocardial tissue, as well as the regeneration ratio, spatial localization, and functional differences of LEC subgroups after MI, we deduced that LEC ca III may be involved in the direct regulation of myocardial injury in the IZ from the perspective of metabolic stress, whereas LEC ca II may be related to the rapid immune inflammatory response in the BZ in the very early stages of MI. LEC ca I and LEC co primarily participate in the regulation of myocardial tissue edema resolution in the middle and late stages post-MI.

2.4 Single-Cell Trajectories of LECs Subsets post-MI

How do LEC subgroups regenerate and evolve after MI? To answer this question, we used cell trajectory analysis to characterize LECs development and determine lineage differentiation. From the pseudo-time plot and phenotype-based trajectory plot, we learn that, in the early stage post-MI, the main LEC subgroup is still LEC ca II and III, which is consistent with the spatial transcriptome localization results. LEC ca II was significantly upregulated in the BZ and RZ of the infarcted area, and Ca III was significantly upregulated in the IZ. During the mid-to-late stages, we found that LEC ca II gradually differentiated into two orientations. One group was mainly composed of ca I, which may regulate immune and metabolic outcomes, while the other group jointly involved ca I, ca III, and co, which may be mainly involved in cell death, inflammation and edema regression (Figures. 4A-C). These results further suggest that ca II and III mainly participate in the early stages of

178 myocardial infarction, whereas ca I and co are involved in the regulation of injury repair in the
179 middle and late stages after MI.

180 What are the main regulatory molecules in these LEC subgroups during pseudo-time post-MI?
181 Subsequently, we screened and performed KEGG functional enrichment analysis on temporally
182 expressed genes during MI and obtained four gene sets (Figures. 4D and 4E). Interestingly, these
183 genes corresponded well with the ratios of different LEC subgroups during MI (Figure 4F). Gene
184 set 1, similar to LEC ca III, which is highly expressed at the very early stages of MI and then
185 gradually decreases, is mainly related to oxidative phosphorylation, diabetic cardiomyopathy,
186 cholesterol metabolism, thermogenesis, and the peroxisome proliferator activated receptor (PPAR),
187 cyclic guanosine 3', 5'- monophosphate (cGMP) - Protein Kinase G (PKG) signaling pathway. The
188 expression of gene sets 2 and 3 was lower during MI, significantly increased in the early and middle
189 stages, and gradually decreased thereafter. These genes are primarily involved in the regulation of
190 programmed cell death, apoptosis, amino acid metabolism, glycolysis, and gluconeogenesis. Gene
191 set 4 showed lower expression in the early stage of myocardial infarction, but gradually increased
192 in the middle and showed the highest expression in the late stages post-MI. These genes are mainly
193 involved in cardiac regeneration, renin secretion, bicarbonate reabsorption, salivary and bile
194 secretion, as well as parathyroid and growth hormone synthesis and secretion. These results imply
195 that LECs are mainly involved in the stress regulation of cell metabolism, inflammation, and death
196 in the very early stages of MI, while regeneration and repair functions are mainly involved in the
197 late stages.

198 **2.5 Assessment of Cell-Cell Communication**

199 To explore how lymphocytes and immune cells interact to regulate metabolic inflammation in the
200 early stages of MI, we conducted further clustering analysis on immune cells from the RAW Data
201 (E-MTAB-7895). As shown in Figure5 -figure Supplement 1A and 1B, seven immune cell types
202 were identified: neutrophils (S100a8 and S100a9), monocytes I (Chil3 and Plac8) and II (Saa3 and
203 Arg1), macrophages (C1qa and Cd68), dendritic cells (H2ab1 and Cd74), B cells (Cd79a and Igkc),
204 and natural killer T cells (Nkg7 and Ms4a4b). The R Package "CellChat" was used to investigate
205 the communication and interaction between these cells and LEC subpopulations. As expected, the
206 communication strength of all significant signaling pathway analyses showed that the highest level
207 of communication probability occured between LEC ca I, NKT and B cells in normal heart tissue,
208 as shown in Figure 5A. During the early phase of MI, that is, between D1 and D3, the highest
209 interaction numbers and strength found were between LEC ca I and ca III, as well as monocytes and
210 macrophages (Figure 5A). Next, correlation analysis was conducted on the strength of the receptor-
211 ligand of LEC and immune cells, except for the classical APP-CD74 pathway (MHCII, expressed
212 by activated APC cells); the interaction was found to be more active in the Galectin9-CD44 and
213 CD45, as well as Collagen-CD44, and ICAM1-ITGβ2 pathways, between the LEC ca I and III, as
214 well as monocytes type I or macrophages ($P<0.05$) (Figures. 5B and 5C; Figure5-figure Supplement
215 1C and 1D). This indicates that monocytes and macrophages may be the key immune inflammatory
216 cells that regulate lymphocyte immune presentation during the early phases of MI.

2.6 Factors Mediating LECs that Regulate Myocardial Edema post-MI.

In this study, we reveal that fluid retention, one of the basic functions of lymphatic vessels, occurs in LEC ca I and LEC co in the middle-late phase of MI. Therefore, we explored all molecules that may have important regulatory effects on edema regression. Through localization and temporal expression analysis of KEGG pathway genes in the lymphocyte subpopulation, the expression of Aquaporin 1(AQP1) in LEC was found to be significantly correlated with temporal changes in edema occurrence and resolution (Figure 6A). Furthermore, the score of the degree of tissue edema in cardiac tissue post-MI, was analyzed and the mouse heart was found to rapidly develop edema on D1 after MI, with the edema reaching its maximum on D3. The edema gradually decreased on D7, and returned to normal on D14 (Figures. 6B and 6C). This was negatively correlated with the expression level of AQP1 in LEC after myocardial infarction. IF co-staining of AQP1 and LVEC in heart tissue also revealed that the expression of AQP1 was significantly reduced in the early phase of MI D1 and D3, and markedly increased expressed in MI D7 and D14 post-MI (Figure 6D). mLECs (cultured mouse LEC cell line) was used and $CoCl_2$ intervention (simulated hypoxia stimulation) was found to reduce the expression of AQP1 at both the transcriptional and expression levels in a dose-dependent manner (Figures. 6E-6J). These results suggest that AQP1 may be involved in the regulation of lymphatic edema metabolism after MI. Early intervention or increased gene expression may improve cardiac function in MI.

2.7 Influence of LEC on Infiltration of Macrophages Via the Galectin9-CD44 Pathway

To clarify whether the Galectin9(Gal9)-CD44 axis is involved in the regulation of the interaction between LECs and monocyte-macrophages in the early stages of MI, we looked for the temporal expression changes of Gal9 in LECs post-MI. Consistent with the results of the bioinformatics analysis, Gal9 was highly expressed in LECs D3 and D7(Figure 7A), whereas CD44 expression gradually decreased from D1(Figure 7B). Further in vitro studies have found that Gal9 expression was significantly increased in a dose-dependent manner in IFNγ-stimulated cultured mLECs but not hypoxia-stimulated cells (Figures. 7C-7E). Moreover, intervention with recombinant Gal9 significantly induced macrophage migration in a dose-dependent manner (Figures. 7F-7H). In contrast, the inhibition of Gal9 expression significantly inhibited interferon regulated macrophage migration (Figures. 7I-7M). These results further clarify that LECs may participate in the regulation of myocardial tissue immune inflammation through the Gal9-CD44 axis in the early stages of MI.

3 Discussion

This study reveals, for the first time, the dynamic transcriptional heterogeneity distribution of myocardial lymphatic vessels in different regions of myocardial tissue post-MI, these vessels were shown to form different functional subgroups that exhibit different bioeffects in the myocardial tissue post-MI. Following this, a preliminary overview of cardiac lymphatics in infarcted heart at transcriptional level was obtained and the lymphatic system was concluded to be involved in cardiac repair post-MI.

The lymphatic system plays an essential role in interstitial fluid balance and immune cell hemostasis in many organs(Petrova & Koh, 2020), including the heart(Brakenhielm & Alitalo, 2019). Stimulating lymphangiogenesis post-MI was found to alleviate myocardial edema and improve heart function(Henri et al., 2016; Houssari et al., 2020; Trincot et al., 2019). Henri et al(Henri et al., 2016) observed lymphangiogenesis and heart function at 4 and 12 weeks post-MI, and found reduced myocardial edema and fibrosis in VEGFC stimulated mice as compared to the control group. However, lymphangiogenesis in the natural pathological process post-MI, especially in the early stage post-MI, was not observed in this study. Generally, myocardial edema and inflammation are occurred in MI early stage, what does cardiac lymphatics changed simultaneously caught our interest. So we established mice MI model to observe the physiological and pathological changes in cardiac lymphatics. Interestingly the rate and morphology of lymphatic vessel neogenesis were found to vary in different zone of the infarcted heart, and several large, dilated, continuous Lyve1-labeled lymphatic vessels appeared along the middle myocardium quickly in the border zone in D7 post-MI，which was mainly observed in epicardium and endocardium in the normal heart, this abnormal remolding indicate their new role in this pathological scenario.

Takeda et al(Takeda et al., 2019) have unveiled LEC heterogeneity and their function in human lymphatics, dividing LEC into six subtypes, and found that CD209 on medullary sinuses LECs mediates neutrophil adhesion in the human lymphatic node medulla. Lymphatic vessels LECs, however, have been teeny elaborated. In this study, LECs of lymphatic vessels were clustered into one collecting LEC and three capillary LEC, and, after localized them in space, found that each subtype focuses on different functions in infarcted heart. LEC ca II and III mainly participate in inflammation in the early stage post-MI in the RZ and IZ, while ca I and co are involved in the regulation of myocardial edema in the middle and late stages after MI in the BZ and IZ. In addition to these traditional roles in immune regulation and interstitial fluid hemostasis, LEC capillaries, especially LEC ca III, also participate in metabolic regulation(glycolysis and gluconeogenesis), which might provide energy for immune cell migrantion or myocardium survival(Guak & Krawczyk, 2020; Zuurbier et al., 2020).

Previous studies have reported that lymphangiogenesis stimulation post-MI can suppress T-cell infiltration and reduce infarct thinning(Houssari et al., 2020), and that activated LECs penetrating the infarcted heart increase the number of tolerogenic dendritic cells and regulatory T cells, thereby inhibiting the expansion of NKT cells and promoting reparative macrophage expansion to facilitate post-MI repair(Wang et al., 2023). This provides a clue for the treatment of lymphatics in infarcted heart.

Herein, we also identified some interesting findings from the cell-chat analysis between LEC and immune cells. We found that LECs were mainly involved in the chemotactic function of neutrophils, monocytes, and macrophages during the early stages of MI. Macrophage chemotaxis not only participates in the inflammatory response after myocardial infarction, but may also serve as an important immune presenting cell involved in the immune regulation of LEC in myocardial tissue after MI. Second, we found that LEC could regulate monocyte and macrophage infiltration through the Galectin9-CD44 pathway. Galectin9 release from LEC in hypoxia is reduced, which slows

macrophage migration, increased Galectin9 in the medium of the macrophage can accelerates its migration. Galectin 9 is one of the β-galactoside binding lectins known for its immunomodulatory role in various microbial infections(Moar & Tandon, 2021), it has been reported that serum Galectin 9 levels are associated with the severity of coronary artery disease, and the ST-segment elevation MI patients have the lowest serum level of Galectin9, followed by the non-ST segment elevation MI group and the stable angina groups(Zhu et al., 2015). Therefore, galectin9 may be a potential molecule involved in controlling the inflammation response post-MI.

Moreover, we screened out a key edema regulated gene, Aqp1, which is highly expressed in LEC subsets in the middle and late phases of MI. Aqp1 is expressed in many tissues, and its primary function is transmembrane water flux(Trillo-Contreras, Toledo-Aral, Echevarría, & Villadiego, 2019). A previous study showed that the knockout of the Aqp1 gene can result in impaired urine concentration(Z. Qiu, Jiang, Li, Wang, & Yang, 2023) and lung edema(Bai et al., 1999) in mouse model. We showed that Aqp1 expression decreased at both the RNA and protein levels in mouse LECs under hypoxic stimulation, and that its expression was negatively correlated with myocardial edema in LECs post-MI. This suggests that Aqp1 may be an essential factor in myocardial edema and needs to be elucidated, along with the underlying mechanism.

In conclusion, LECs play an important role in regulating myocardial edema and inflammation post-MI, and stimulation of lymphangiogenesis or promotion of LEC function may become new targets for future clinical improvement of cardiac function post-MI. One limitation of this study is that the single-cell sequencing data that were analyzed for each time point was derived from a single sample, which resulted in resultant LEC counts being too small. This might have resulted in bias in the analyses. In future studies, multiple samples should be utilized to improve the yield of trace cells like LEC for single cell sequencing. Therefore, further validation tests must be designed and implemented.

4 Materials and Methods

4.1 Animals and MI model

All animal care and experimental procedures were approved by the Department of Cardiology of the General Hospital of Northern Theater Command and the Cardiovascular Research Institute of the PLA, in accordance with the National Institutes of Health regulations on the use of laboratory animals. Eight-week-old male C57BL/6J mice were obtained from the GemPharmatech Co., Ltd (Nanjing, China). Myocardial infarction Models established by ligation of the left anterior descending artery methodology referred to published study (Liu et al., 2021).

4.2 Ultrasound Assessment of Cardiac Function

Ultrasonography was performed using a small animal ultrasound imaging system (Vevo 2100, FUJIFILM VisualSonics, Canada) equipped with a 30 MHz linear ultrasonic transducer. The animals were anesthetized with 2% isoflurane during the ultrasound. The observer who performed

330 the investigation was blinded to the experimental groups. The main cardiac structural and functional
331 measurements were referred to the published study(Liu et al., 2021).

332 **4.3 Immunofluorescence and Quantification of Lymphatics**

333 Mice hearts were harvested and postfixed in 4°C 4% paraformaldehyde(PFA) for 4 hours, following
334 dehydration in 4°C 30% sucrose solution overnight, then 4μm frozen slices were sectioned after
335 OCT embedded. Hematoxylin & Eosin staining was performed under standard procedures. For
336 Immunofluorescence(IF), frozen section were blocked with 5% normal goat serum (BioGenex,
337 Fremont, CA) at room temperature for 1hour, and then stained with primary antibodies including,
338 rabbit anti-Lyve1 (1:300, ab14917, Abcam, UK), rabbit anti-Prox1(1:300, ab199359, Abcam, UK)
339 and mouse anti-Aqp1(1:300, sc-25287, Santa, USA) overnight at 4°C, Alexa Fluor 488- or 595-
340 conjugated secondary antibodies including, wheat germ agglutinin (WGA) (1:500, Sigma-Aldrich)
341 in the dark for 1 hours at room temperature on secondary morning. After 5 minutes 4',6-diamidino-
342 2-phenylindole (DAPI)(Invitrogen USA) staining for cell nuclei, images were captured using a
343 confocal microscope (LSM800; Carl Zeiss Microscopy Ltd, Cambridge, MA). For quantification of
344 vessel area, vessels with visible lumens were measured using Image J. Five equally sized
345 measurement areas were selected in respective zone (remote zone, infarct zone and border zone) of
346 each slice.

347 **4.4 Edema Quantification**

348 Edema quantification from histology images of cardiac paraffin sections were referred to the
349 published study(Trincot et al., 2019). Fourty high-power (40X) representative images were chosen
350 per animal; each image must have a clear border of the section visible. Images were blinded and
351 scored by two independent observers (Score 1=no edema, 2=mild edema, 3=severe edema). Graphs
352 represent the average score value per animal.

353 **4.5 Cell culture**

354 The mouse lymphatic endothelial cell line(mLECs) was gifted by Prof. Lin Chen (Army Medical
355 University, China). Mouse monocyte macrophage(J774A.1) was purchased from FuHeng Cell
356 Center (Shanghai, China). All the cell lines were cultured in DMEM with 10% fetal bovine
357 serum(VivaCell Biosciences, China) and 1% antibiotics(penicillin and streptomycin) (Sangon
358 Biothec, China) at 37°C.

359 **4.6 Cell transfection**

360 Small interfering RNAs(SiRNAs) were purchased from GenePharma (Shanghai, China). The
361 sequences of SiRNA-NC and SiRNA-Lgals9 are listed in **Table S1**. SiRNA were transfected into
362 cells using Transfection Reagent (0000002157, PolyPlus, France) when LEC cell had 40-60%
363 confluence. The efficiency of transfection was detected by RT-qPCR and WB after transfection.

364 **4.7 Cell Migration Test**

365 Cell migration was measured by wound healing assay and transwell assay. Wound healing assay
366 procedure were referred to the published study(Martinotti & Ranzato, 2020). For transwell assay,
367 2.5×10^4 J774A.1 cells were inoculated into the upper chamber and cultured in serum-free medium.
368 The lower cavity contains 20% fetal bovine serum DMEM medium with or without LEC cocultured.
369 After 24 hours, the migrated cells were immobilized with methanol and stained with 0.1% crystal
370 violet solution (Solarbio, China) at room temperature for 20 minutes. The number of migrating cells
371 was quantified by counting the number of cells in 10 random fields under a 40X magnifying glass.

372 **4.8 Western Blotting**

373 mLEC were lysed in RIPA buffer (UJ289235, Thermo Fisher Scientific, USA). Equal amounts of
374 protein were separated by SDS-PAGE (120 V for 1 h) and then transferred onto a polyvinylidene
375 difluoride membrane (R9KA84149, Merck Millipore Ltd. Germany). The membranes were then
376 incubated with the following primary antibodies at 4 °C overnight: mouse anti-Aqp1 (1:1000, sc-
377 25287, Santa, USA), rabbit anti-Gal9 (1:1000, ab69630, Abcam, UK) and rabbit anti-GAPDH
378 (1:1000, CST, USA). After incubation, the membranes were washed and incubated with goat anti-
379 rabbit IgG (1:2000, 150783, Jackson ImmunoResearch, USA) for 1h at room temperature. Finally,
380 the protein bands of the membranes were detected by chemiluminescence with ECL (BIO-RAD,
381 USA). The WB bands were quantitated via the software ImageJ.

382 **4.9 Real-Time PCR**

383 Total RNA from mLEC was extracted using the TRIzol reagent (Thermo Fisher Scientific, USA).
384 The isolated RNA was converted into cDNA using the PrimeScript RT with gDNA Eraser kit (Takara,
385 Japan). Quantitative real-time PCR was performed using SYBR1 Premix Ex Taq II (Takara, Japan).
386 The sequences of primers (forward and reverse) are presented in **Table S2.**

387 **4.10 Data Collection**

388 Single-cell transcriptomic data was retrieved from ArrayExpress(E-MTAB-7895). Single-cell
389 nucleus transcriptomic data and spatial transcriptomic were retrieved from the Gene Expression
390 Omnibus (GEO; https://www.ncbi.nlm.nih.gov/geo/) database(GSE214611).

391 **4.11 scRNA Analysis**

392 The E-MTAB-7895 data set provided this study with filtered data for 0, 1, 3, 7, 14, and 28 days
393 post-MI. After downloading the matrices, downstream analysis was performed using the Seurat
394 package (version 4.3.0)(Hao et al., 2021) in R (version 4.1.3; R Foundation). Dimension reduction
395 was performed using principal-component analysis (PCA) with the RunPCA function and the
396 optimal number of principal components (PCs) was selected using the ElbowPlot function. The
397 same PCs were also applied to cell clustering with modularity optimization using the kNN graph

algorithm as the input. Cell clusters were visualized using the uniform manifold approximation and projection(UMAP) algorithm. The cell types were annotated based on the expression of known marker genes, as previously described. Marker genes for each cell type were obtained using the Seurat function FindAllMarkers, in which only markers with positive log2-transformed fold changes were considered. Differentially expressed genes (DEGs) in each cluster were then identified using the Wilcoxon test.

To characterize the process of LEC cell development and determine lineage differentiation among diverse LEC cells, cell trajectory analysis was conducted using single-cell pseudo-time trajectories constructed with the Monocle2 package (v2.22.0),(X. Qiu et al., 2017) according to the provided documentation (http://cole-trapnell-lab.github.io/monocle-release/). UMI counts were modeled as a negative binomial distribution; ordering genes were identified as having high dispersion across cells (mean_expression≥0.01; dispersion_empirical≥1). The discriminative dimensionality reduction with trees (DDRTree) method was used to reduce data to two dimensions. Gene sets identified from the destination analysis were clustered and visualized using the plot_genes_in_pseudotime function.

The differences in putative cell-cell communication modules between cell types were analyzed for the samples at each stage. The Cellchat (v1.6.1) package includes a comprehensive signaling molecule interaction database that considers the known structural composition of receptor-ligand interactions, such as multimeric receptor-ligand complexes, soluble agonists and antagonists, as well as stimulatory and inhibitory membrane-bound coreceptors(Jin et al., 2021). The inference of cell-cell interactions includes the identification of differentially expressed signaling genes, calculation of ensemble average expression and intercellular communication probability, as well as identification of statistically significant intercellular communications. The single-cell transcriptomic data was divided into seven parts according to the stages and the differences in ligand-receptor interactions and signaling pathways, were explored across these seven stages.

4.12 Spatial Localization of LEC Cells

Single nucleus and spatial transcriptome data at 1h, 3 days, and 7days were downloaded. Categorical or continuous data were transferred across single-cell datasets. Briefly, for each sample, the gene-spot matrix and snRNA matrix were normalized by SC transformation and dimensionality reduction was performed by PCA. To transfer categorical information, a vector was pass through the reference dataset. Next, a set of anchors in the scRNA, snRNA and ST data were identified, which were subsequently transferred to query objects using the FindTransferAnchors and TransferData functions in Seurat.

4.13 Statistic analysis

Data are presented as mean±standard error of mean(SEM). All data were analyzed using SPSS version 22.0 (SPSS, Chicago, IL, USA), and graphs were prepared using GraphPad Prism 8(GraphPad Software, CA, USA). Differences between two groups were evaluated using an

unpaired Student's t-test. Differences among three or more groups were evaluated using one-way analysis of variance (ANOVA). Statistical significance was set at $P<0.05$.

5 Data availability

Data been analyzed in this study is publicly available from ArrayExpress(E-MTAB-7895) and the Gene Expression Omnibus (GEO; https://www.ncbi.nlm.nih.gov/geo/) database(GSE214611).

6 Conflict of Interest

None

7 Author Contributions

YLH and CHY contributed to the conception and made final approval of the version; JQH and DLZ performed the study concept, wrote the manuscript, and performed the experiment; HXS, ZQL, DL, XLZ, XJZ, YZ, JL, and JXX helped with the experiment and data analysis. All authors contributed to the manuscript revision, read and approved the submitted version.

8 Funding

This work was supported by the National Natural Foundation of China (8220022542,82270300 and 82200431), The Liaoning Science and Technology Project (2022JH2/101300012)

9 References

Alitalo, K. (2011). The lymphatic vasculature in disease. *Nat Med, 17*(11), 1371-1380. doi:10.1038/nm.2545

Alitalo, K., Tammela, T., & Petrova, T. V. (2005). Lymphangiogenesis in development and human disease. *Nature, 438*(7070), 946-953. doi:10.1038/nature04480

Anzai, A., Ko, S., & Fukuda, K. (2022). Immune and Inflammatory Networks in Myocardial Infarction: Current Research and Its Potential Implications for the Clinic. *Int J Mol Sci, 23*(9). doi:10.3390/ijms23095214

Bai, C., Fukuda, N., Song, Y., Ma, T., Matthay, M. A., & Verkman, A. S. (1999). Lung fluid transport in aquaporin-1 and aquaporin-4 knockout mice. *J Clin Invest, 103*(4), 555-561. doi:10.1172/jci4138

Brakenhielm, E., & Alitalo, K. (2019). Cardiac lymphatics in health and disease. *Nat Rev Cardiol, 16*(1), 56-68. doi:10.1038/s41569-018-0087-8

Bulluck, H., Dharmakumar, R., Arai, A. E., Berry, C., & Hausenloy, D. J. (2018). Cardiovascular Magnetic Resonance in Acute ST-Segment-Elevation Myocardial Infarction: Recent Advances, Controversies, and Future Directions. *Circulation, 137*(18), 1949-1964.

466 doi:10.1161/circulationaha.117.030693
467 Chen, R., Zhao, H., & Yan, H. (2022). Long-term Management of Patients with Myocardial Infarction:
468 An Updated Review. *2*(4), 241-262. doi:10.1097/cd9.0000000000000073
469 Grün, D., & van Oudenaarden, A. (2015). Design and Analysis of Single-Cell Sequencing Experiments.
470 *Cell, 163*(4), 799-810. doi:10.1016/j.cell.2015.10.039
471 Guak, H., & Krawczyk, C. M. (2020). Implications of cellular metabolism for immune cell migration.
472 *Immunology, 161*(3), 200-208. doi:10.1111/imm.13260
473 Hao, Y., Hao, S., Andersen-Nissen, E., Mauck, W. M., 3rd, Zheng, S., Butler, A., . . . Satija, R. (2021).
474 Integrated analysis of multimodal single-cell data. *Cell, 184*(13), 3573-3587.e3529.
475 doi:10.1016/j.cell.2021.04.048
476 Henri, O., Pouehe, C., Houssari, M., Galas, L., Nicol, L., Edwards-Lévy, F., . . . Brakenhielm, E. (2016).
477 Selective Stimulation of Cardiac Lymphangiogenesis Reduces Myocardial Edema and Fibrosis
478 Leading to Improved Cardiac Function Following Myocardial Infarction. *Circulation, 133*(15),
479 1484-1497; discussion 1497. doi:10.1161/circulationaha.115.020143
480 Heron, C., Ratajska, A., & Brakenhielm, E. (2022). Cardiac lymphatics: state of the art. *Curr Opin*
481 *Hematol, 29*(3), 156-165. doi:10.1097/moh.0000000000000713
482 Houssari, M., Dumesnil, A., Tardif, V., Kivelä, R., Pizzinat, N., Boukhalfa, I., . . . Brakenhielm, E. (2020).
483 Lymphatic and Immune Cell Cross-Talk Regulates Cardiac Recovery After Experimental
484 Myocardial Infarction. *Arterioscler Thromb Vasc Biol, 40*(7), 1722-1737.
485 doi:10.1161/atvbaha.120.314370
486 Huang, L. H., Elvington, A., & Randolph, G. J. (2015). The role of the lymphatic system in cholesterol
487 transport. *Front Pharmacol, 6*, 182. doi:10.3389/fphar.2015.00182
488 Huang, L. H., Lavine, K. J., & Randolph, G. J. (2017). Cardiac Lymphatic Vessels, Transport, and Healing
489 of the Infarcted Heart. *JACC Basic Transl Sci, 2*(4), 477-483. doi:10.1016/j.jacbts.2017.02.005
490 Ishikawa, Y., Akishima-Fukasawa, Y., Ito, K., Akasaka, Y., Tanaka, M., Shimokawa, R., . . . Ishii, T. (2007).
491 Lymphangiogenesis in myocardial remodelling after infarction. *Histopathology, 51*(3), 345-
492 353. doi:10.1111/j.1365-2559.2007.02785.x
493 Jin, S., Guerrero-Juarez, C. F., Zhang, L., Chang, I., Ramos, R., Kuan, C. H., . . . Nie, Q. (2021). Inference
494 and analysis of cell-cell communication using CellChat. *Nat Commun, 12*(1), 1088.
495 doi:10.1038/s41467-021-21246-9
496 Klotz, L., Norman, S., Vieira, J. M., Masters, M., Rohling, M., Dubé, K. N., . . . Riley, P. R. (2015). Cardiac
497 lymphatics are heterogeneous in origin and respond to injury. *Nature, 522*(7554), 62-67.
498 doi:10.1038/nature14483
499 Liu, D., Tian, X., Liu, Y., Song, H., Cheng, X., Zhang, X., . . . Han, Y. (2021). CREG ameliorates the
500 phenotypic switching of cardiac fibroblasts after myocardial infarction via modulation of
501 CDC42. *Cell Death Dis, 12*(4), 355. doi:10.1038/s41419-021-03623-w
502 Martinotti, S., & Ranzato, E. (2020). Scratch Wound Healing Assay. *Methods Mol Biol, 2109*, 225-229.
503 doi:10.1007/7651_2019_259
504 Moar, P., & Tandon, R. (2021). Galectin-9 as a biomarker of disease severity. *Cell Immunol, 361*,
505 104287. doi:10.1016/j.cellimm.2021.104287
506 Nahrendorf, M., Pittet, M. J., & Swirski, F. K. (2010). Monocytes: protagonists of infarct inflammation
507 and repair after myocardial infarction. *Circulation, 121*(22), 2437-2445.
508 doi:10.1161/circulationaha.109.916346

Oliver, G., Kipnis, J., Randolph, G. J., & Harvey, N. L. (2020). The Lymphatic Vasculature in the 21(st) Century: Novel Functional Roles in Homeostasis and Disease. *Cell, 182*(2), 270-296. doi:10.1016/j.cell.2020.06.039

Petrova, T. V., & Koh, G. Y. (2020). Biological functions of lymphatic vessels. *Science, 369*(6500). doi:10.1126/science.aax4063

Qiu, X., Mao, Q., Tang, Y., Wang, L., Chawla, R., Pliner, H. A., & Trapnell, C. (2017). Reversed graph embedding resolves complex single-cell trajectories. *Nat Methods, 14*(10), 979-982. doi:10.1038/nmeth.4402

Qiu, Z., Jiang, T., Li, Y., Wang, W., & Yang, B. (2023). Aquaporins in Urinary System. *Adv Exp Med Biol, 1398*, 155-177. doi:10.1007/978-981-19-7415-1_11

Shimizu, Y., Polavarapu, R., Eskla, K. L., Pantner, Y., Nicholson, C. K., Ishii, M., . . . Calvert, J. W. (2018). Impact of Lymphangiogenesis on Cardiac Remodeling After Ischemia and Reperfusion Injury. *J Am Heart Assoc, 7*(19), e009565. doi:10.1161/jaha.118.009565

Takeda, A., Hollmén, M., Dermadi, D., Pan, J., Brulois, K. F., Kaukonen, R., . . . Jalkanen, S. (2019). Single-Cell Survey of Human Lymphatics Unveils Marked Endothelial Cell Heterogeneity and Mechanisms of Homing for Neutrophils. *Immunity, 51*(3), 561-572.e565. doi:10.1016/j.immuni.2019.06.027

Tammela, T., & Alitalo, K. (2010). Lymphangiogenesis: Molecular mechanisms and future promise. *Cell, 140*(4), 460-476. doi:10.1016/j.cell.2010.01.045

Trillo-Contreras, J. L., Toledo-Aral, J. J., Echevarría, M., & Villadiego, J. (2019). AQP1 and AQP4 Contribution to Cerebrospinal Fluid Homeostasis. *Cells, 8*(2). doi:10.3390/cells8020197

Trincot, C. E., Xu, W., Zhang, H., Kulikauskas, M. R., Caranasos, T. G., Jensen, B. C., . . . Caron, K. M. (2019). Adrenomedullin Induces Cardiac Lymphangiogenesis After Myocardial Infarction and Regulates Cardiac Edema Via Connexin 43. *Circ Res, 124*(1), 101-113. doi:10.1161/circresaha.118.313835

Vandereyken, K., Sifrim, A., Thienpont, B., & Voet, T. (2023). Methods and applications for single-cell and spatial multi-omics. *Nat Rev Genet, 24*(8), 494-515. doi:10.1038/s41576-023-00580-2

Vuorio, T., Ylä-Herttuala, E., Laakkonen, J. P., Laidinen, S., Liimatainen, T., & Ylä-Herttuala, S. (2018). Downregulation of VEGFR3 signaling alters cardiac lymphatic vessel organization and leads to a higher mortality after acute myocardial infarction. *Sci Rep, 8*(1), 16709. doi:10.1038/s41598-018-34770-4

Wang, W., Li, X., Ding, X., Xiong, S., Hu, Z., Lu, X., . . . Zhang, Z. (2023). Lymphatic endothelial transcription factor Tbx1 promotes an immunosuppressive microenvironment to facilitate post-myocardial infarction repair. *Immunity, 56*(10), 2342-2357.e2310. doi:10.1016/j.immuni.2023.07.019

Zhu, R., Liu, C., Tang, H., Zeng, Q., Wang, X., Zhu, Z., . . . Zhong, Y. (2015). Serum Galectin-9 Levels Are Associated with Coronary Artery Disease in Chinese Individuals. *Mediators Inflamm, 2015*, 457167. doi:10.1155/2015/457167

Zuurbier, C. J., Bertrand, L., Beauloye, C. R., Andreadou, I., Ruiz-Meana, M., Jespersen, N. R., . . . Krieg, T. (2020). Cardiac metabolism as a driver and therapeutic target of myocardial infarction. *J Cell Mol Med, 24*(11), 5937-5954. doi:10.1111/jcmm.15180

Figure1.

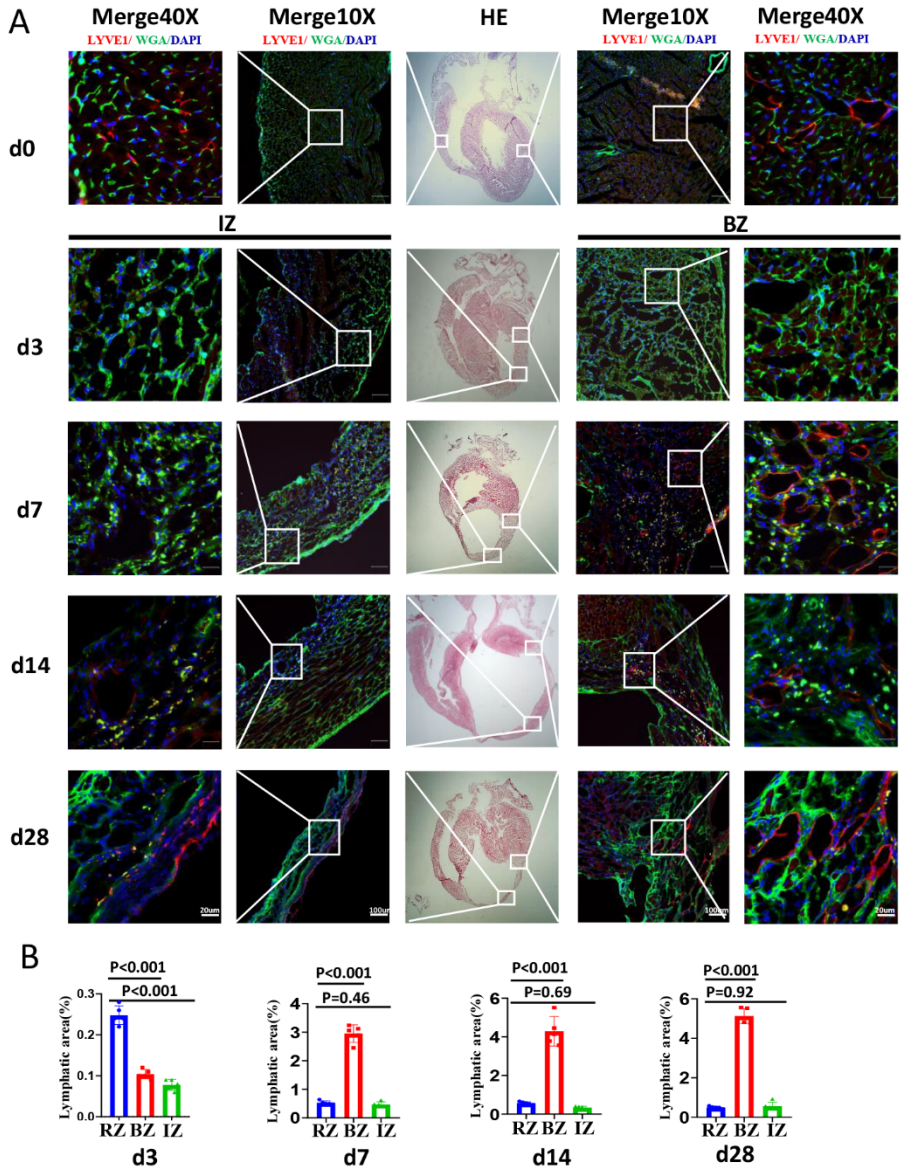

Figure1. Dynamic Changes of Cardiac Lymphatics in Cardiac Tissue post-MI.(A) Hematoxylin-eosin(H&E) stained and immunofluorescence(IF) stained tissue sections in sham and MI models in C57BL/6J mice(n=5~7), LYVE1, lymphatic vessel endothelial hyaluronan receptor 1; WGA: wheat germ agglutinin; DAPI: 4'6-diamidino-2-phenylindole. The scale bar is in 10X:100μm, 40X:20μm.（**B**）Semi-quantitative fluorescence determination of specific regions using ImageJ (n=5 equally sized measurement areas/zone; mean±SEM).

Figure1-figure supplement 1

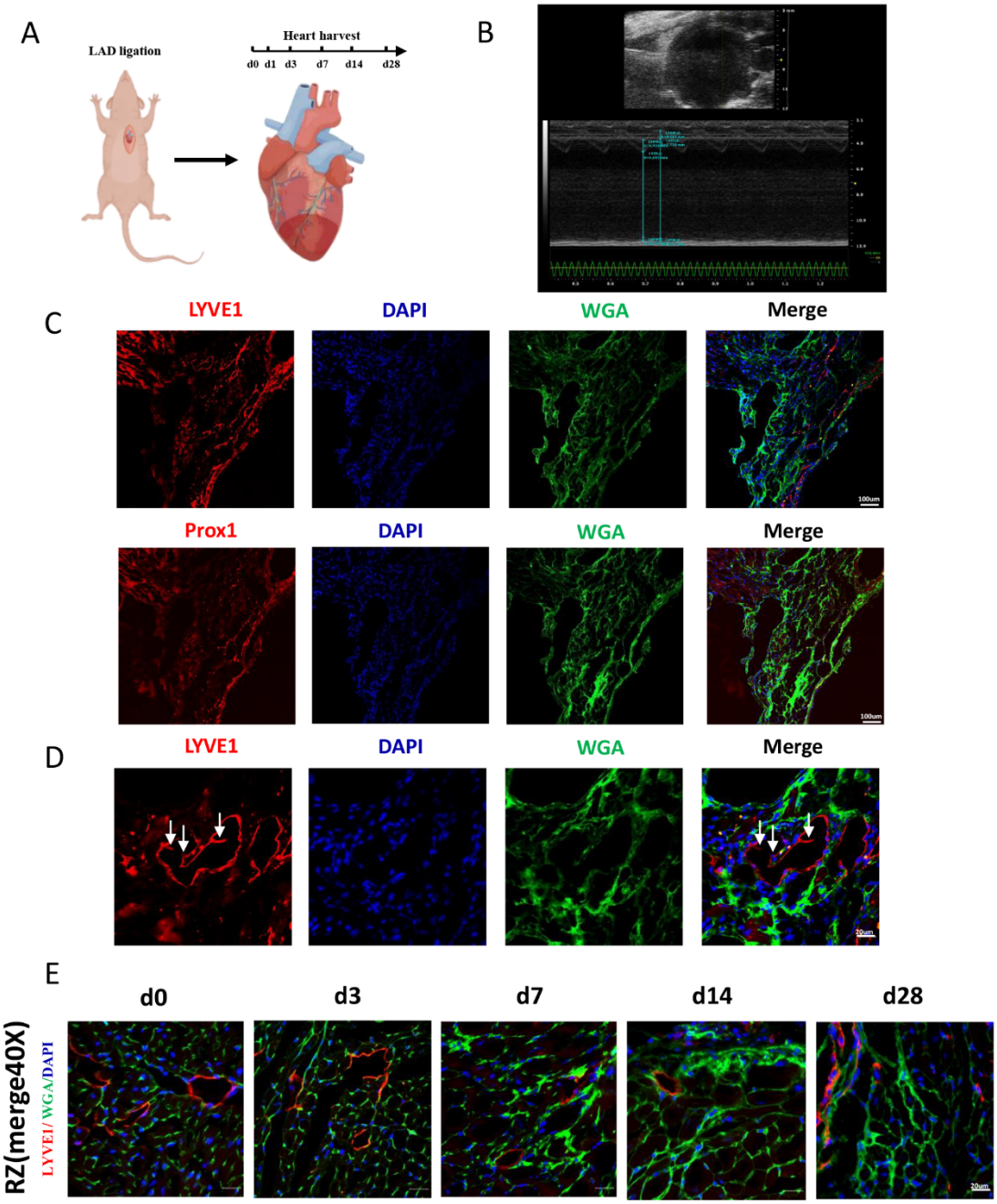

Figure 1-figure supplement 1. (A) Time points for heart harvest after the establishment of the MI models. **(B)**Transthoracic echocardiography confirmation of the MI mouse model. **(C)** Prox1- and Lyve1-labeled cardiac lymphatics in IF-stained frozen tissue section. **(D)** Lyve1-labeled collecting lymphatics with the lymphatic valves highlighted with white arrows. **(E)** IF-stained tissue section of the cardiac lymphatics in the remote zone

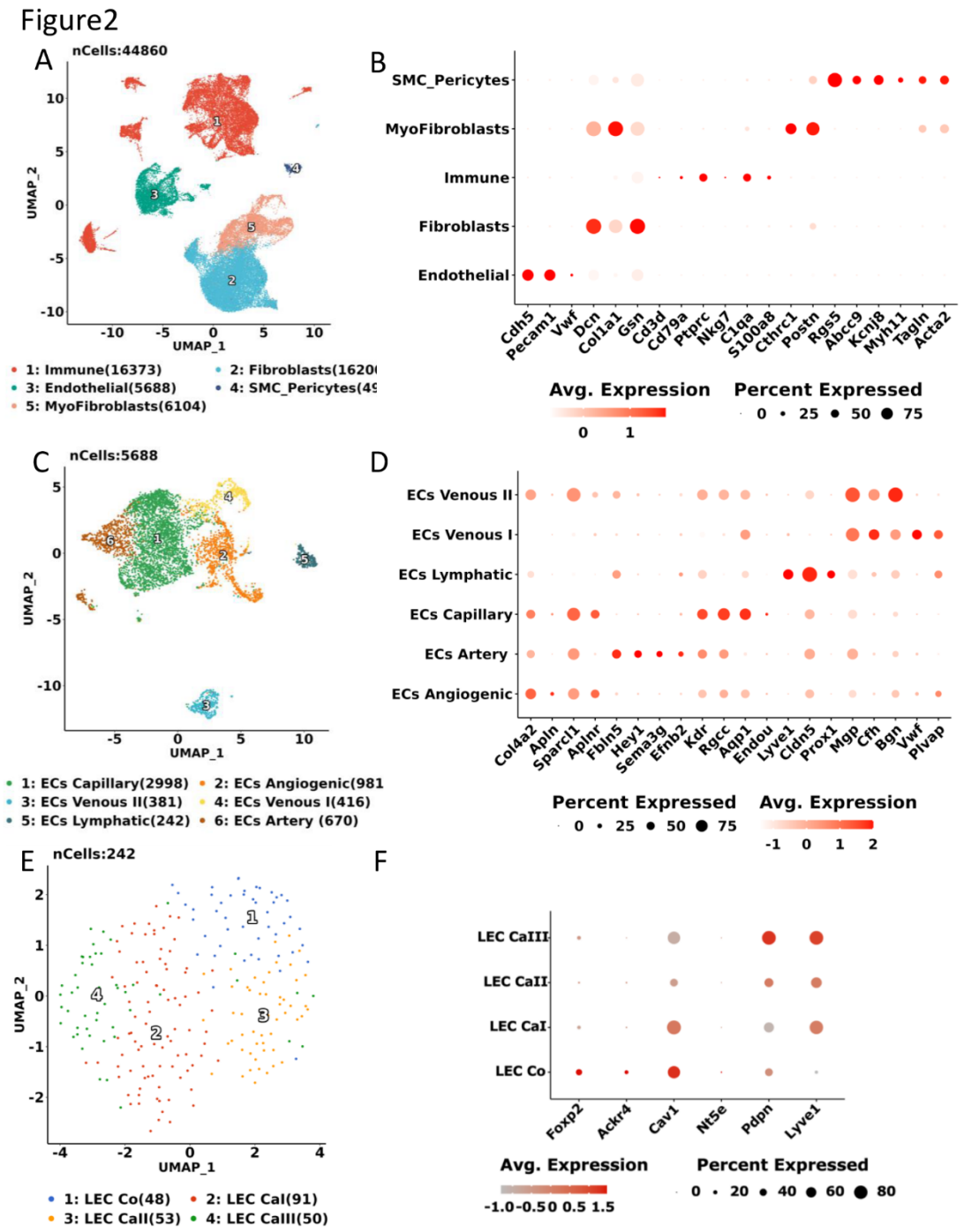

Figure 2. Identificationg of infiltrated cell types in tissues. (A) A Uniform Manifold Approximation and Projection (UMAP) plot of 44,860 cells showing five identified non-myocardium cell types in infarcted heart, cell types are coded with different colors. **(C)** A UMAP plot of single cells profiled in the present work colored by endothelial cell types. **(E)** A UMAP plot of single cells profiled in the present work colored by LEC cell types. **(B, D, and F)** Dot plot showing the average expression of selected cell marker genes. The dots' size and colour indicate the percentage of marker gene expression and the average expression level (Avg. Expression).

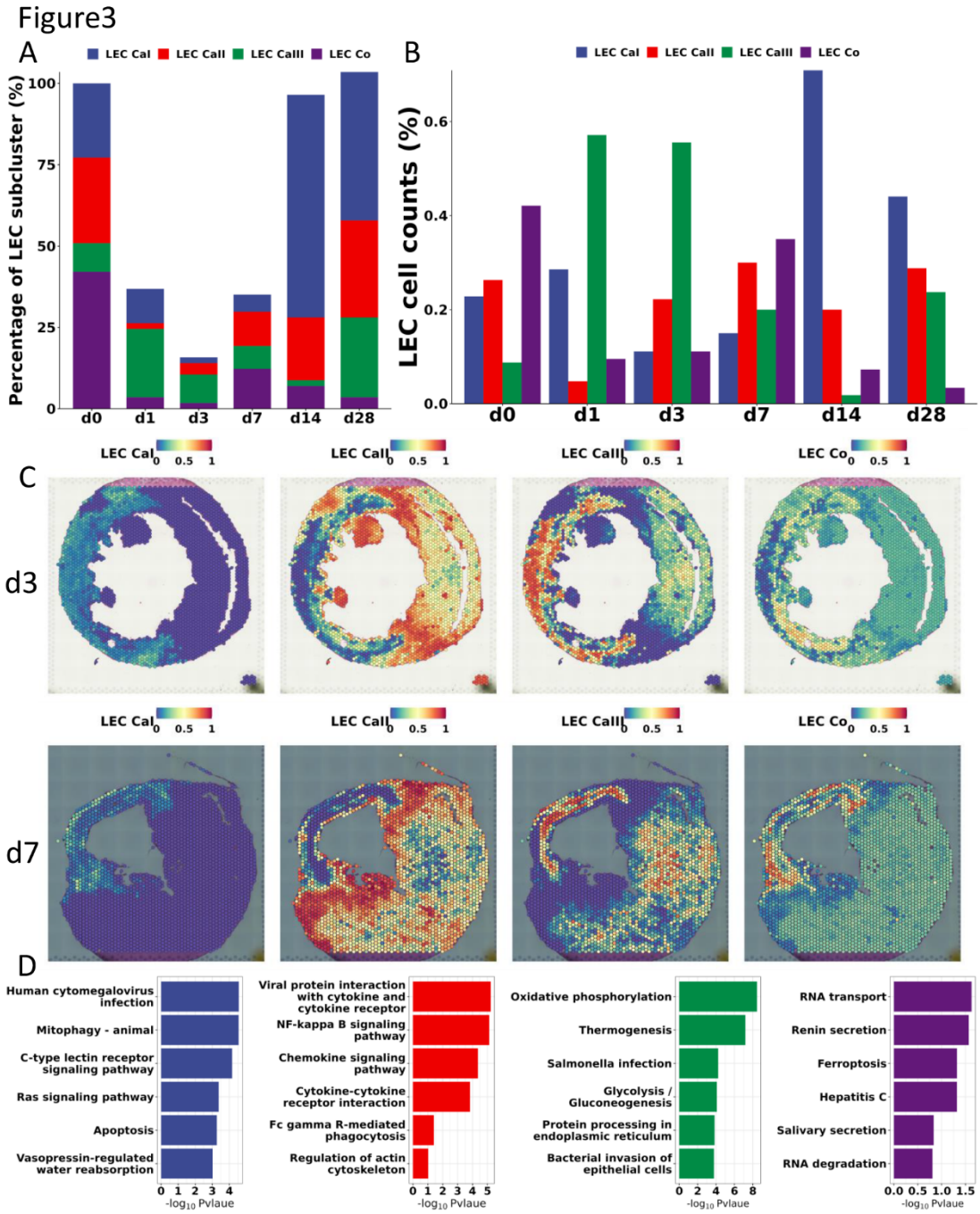

Figure 3. Relationship Between the Spatial Localization and Function of LEC Subpopulations post MI. (A and B) Bar plots showing the proportion of cell types in different samples. **(C)** The proportion of LEC cell types in each spot determined by spatial transcriptome in d3 and d7 post-MI. **(D)** Enriched KEGG pathways of upregulated genes in different LEC cell types, the color indicates the different cell types.

Figure3-figure supplement 1.

A

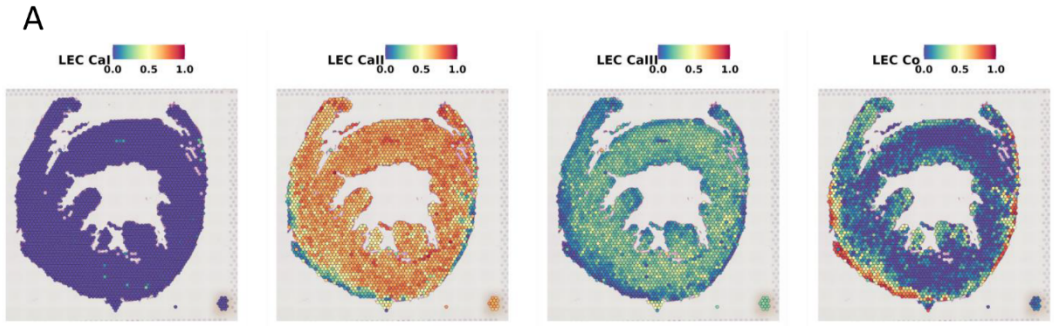

Figure 3-figure supplement 1. (A) The proportion of LEC cell types in each spot was determined via spatial transcriptome analysis in 1 h post-MI.

Figure4

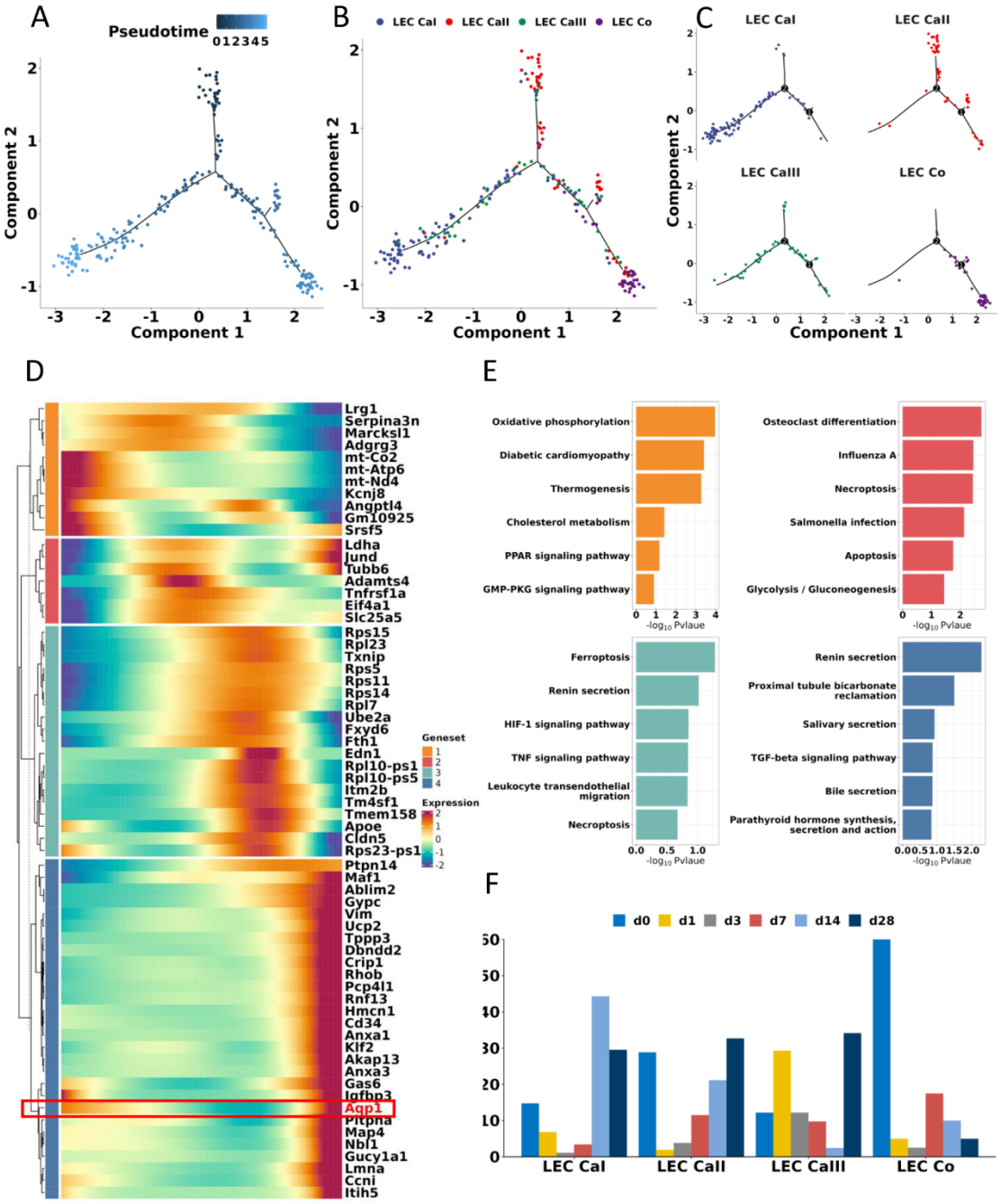

Figure 4. Single-Cell Trajectories of LECs Subsets post MI. **(A, B, and C)** Pseudo-time analysis by Monocle2 shows the potential evolutionary trajectory of LECs, colored by cell types. **(D)** The heatmap shows the set of genes with altered expression levels along the pseudo-time. **(E)** Enriched KEGG pathways in four different gene sets; color indicate different cell types. **(F)** Bar plots showing the proportion of LEC subgroups at different time points.

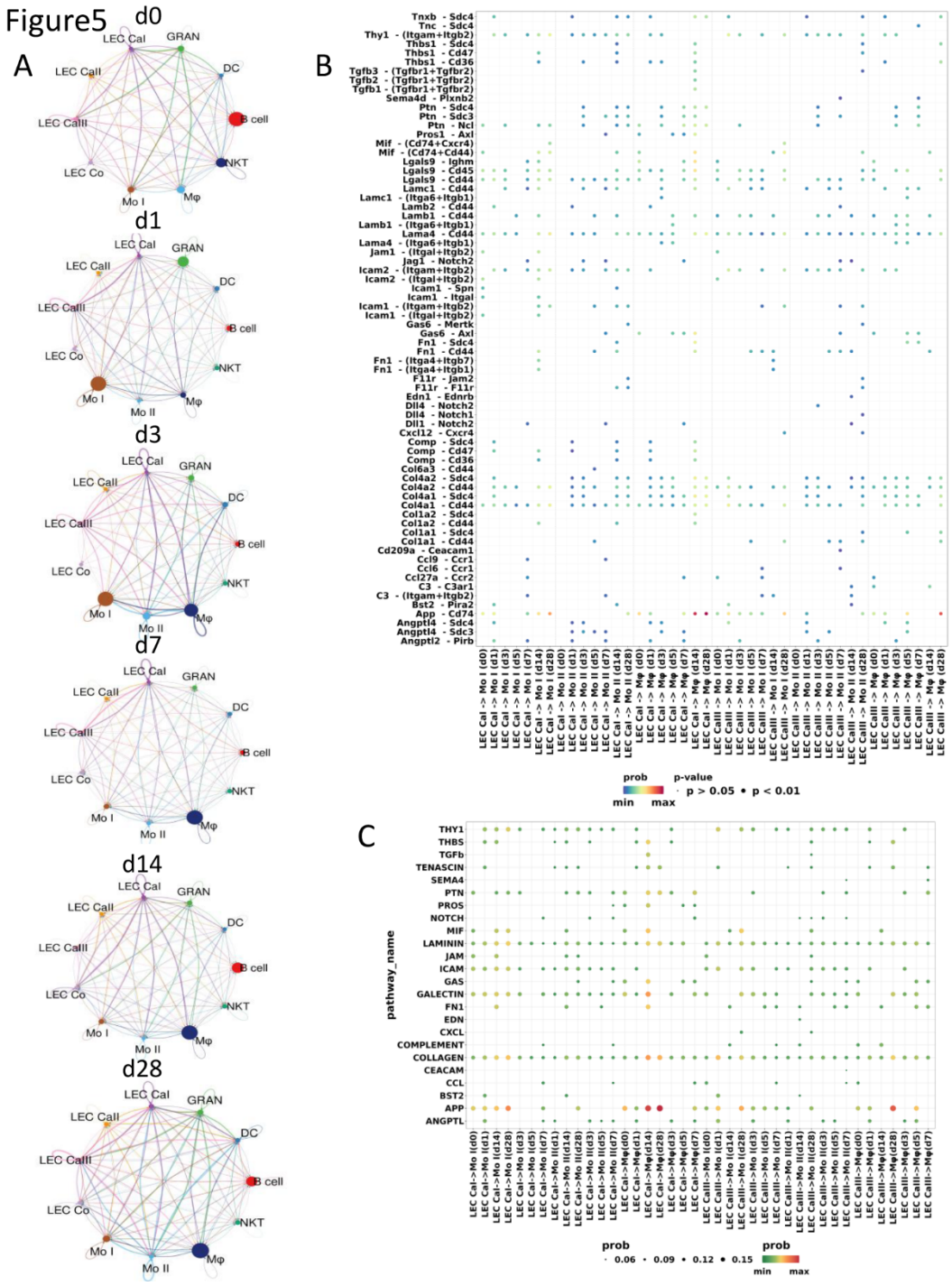

Figure 5. Cell-cell interactions between LECs and immune cells. (A) Interaction net count plot of LECs and immune cells. The thickness of the line represents the number of interactions. **(B)** Bubble plots showing the ligand-receptor pairs originating from LEC ca I and ca III that target monocytes and macrophages, the color indicates the probability of interaction and the size indicates the p-value. **(C)** Bubble plots showing the pathways originating from LEC ca I and LEC ca III that target monocytes and macrophages, the color indicates the probability of interaction and the size indicates the p-value.

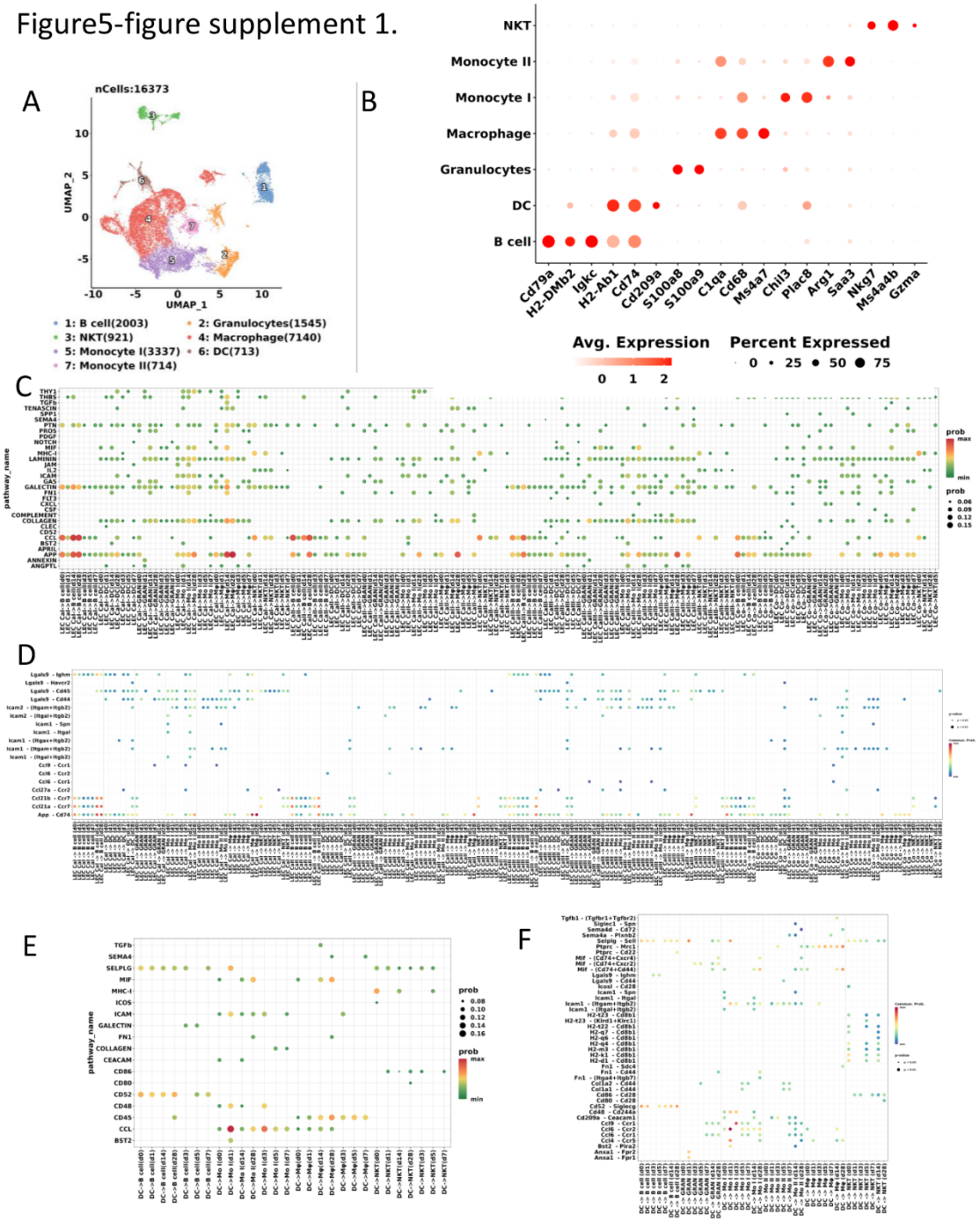

Figure 5-figure supplement 1. (A) A Uniform Manifold Approximation and Projection (UMAP) plot of 16373 cells showing seven identified cell types in immune cells, cell types have been coded with different colors. **(B)** A dot plot showing the average expression of the selected cell marker genes. Dot size and color indicate the percentage of marker gene expression and average expression level (Avg. Expression). **(C)** Bubble plots showing the pathway originating from LECs targeting immune cells; the color indicates the probability of interaction. **(D)** Bubble plots showing the ligand-receptor pairs originating from dendritic cells (DCs) targeting immune cells; the color indicates the probability of interaction and the size indicates the p-value. **(E)** Bubble plots showing the pathways originating from dendritic cells (DCs) targeting other immune cells; color indicates the probability

613 of interaction. **(F)** Bubble plots showing the ligand-receptor pairs originating from dendritic cells
614 (DCs) targeting other immune cells; the color indicates the probability of interaction and the size
615 indicates the p-value.
616

Figure5-figure supplement 2.

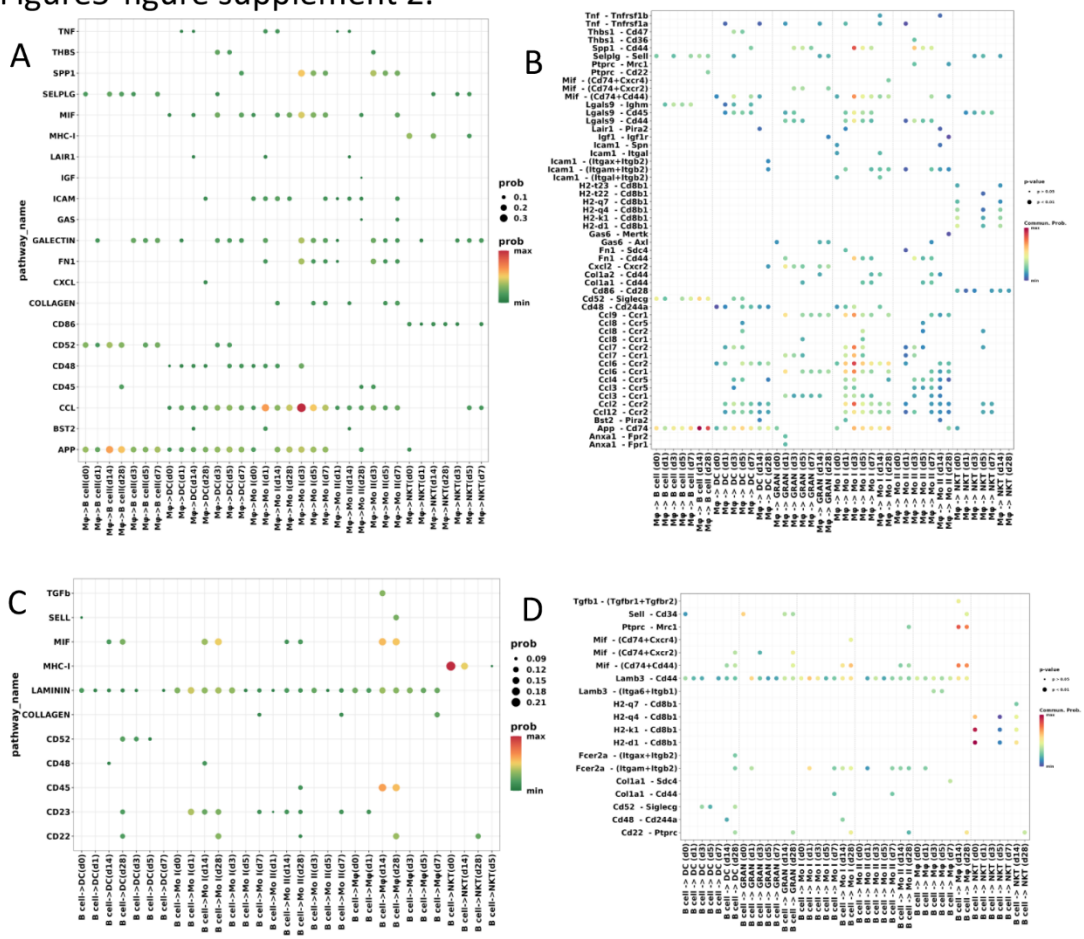

Figure 5-figure supplement 2 (A) Bubble plots showing the pathways originating from the macrophages (Mφ) targeting other immune cells; the color indicates the probability of interaction. **(B)** Bubble plots showing the ligand-receptor pairs originating from Mφ targeting other immune cells; the color indicates the probability of interaction and the size indicates the p-value. **(C)** Bubble plots showing the pathway originating from B cell targeting other immune cells; the color indicates the probability of interaction. **(D)** Bubble plots showing the ligand-receptor pairs originating from B cells targeting other immune cells; the color indicates the probability of interaction and the size indicates the p-value.

Figure6.

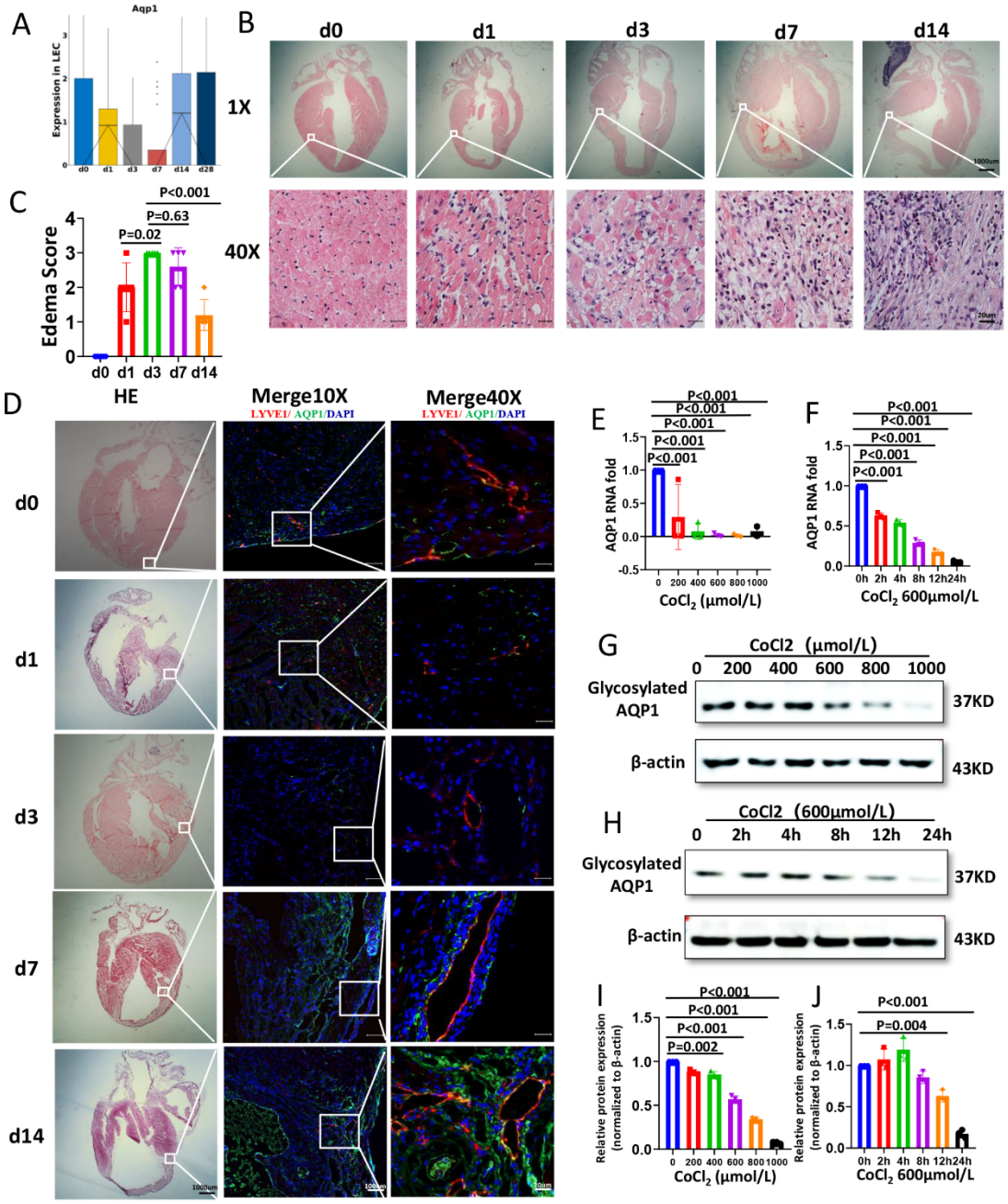

Figure 6. Aqp1 expression on LECs in mouse MI model and on LEC cell line. (A) Expression of Aqp1 gene in LECs at each time point. **(B)** Hematoxylin-eosin(H&E) stained tissue section in sham and MI models of C57 mice(n=5). **(C)** Quantification of the edema in infarcted hearts (n=5). **(D)** H&E stained and immunofluorescence (IF) stained tissue section in sham and MI models of C57 mice (n=5~7), LYVE1, lymphatic vessel endothelial hyaluronan receptor 1; AQP1: aquaporin1; DAPI: 4' 6-diamidino-2-phenylindole; the scale bar is in 10X: 100μm, 40X: 20μm. **(E, and F)** Aqp1 RNA expression in mLEC cell line under $CoCl_2$ hypoxic stimulation over different time points and concentrations. **(G, H, I, and J)** Aqp1 protein expression in mLEC cell line under $CoCl_2$ hypoxic stimulation over different time points and concentrations.

Figure7.

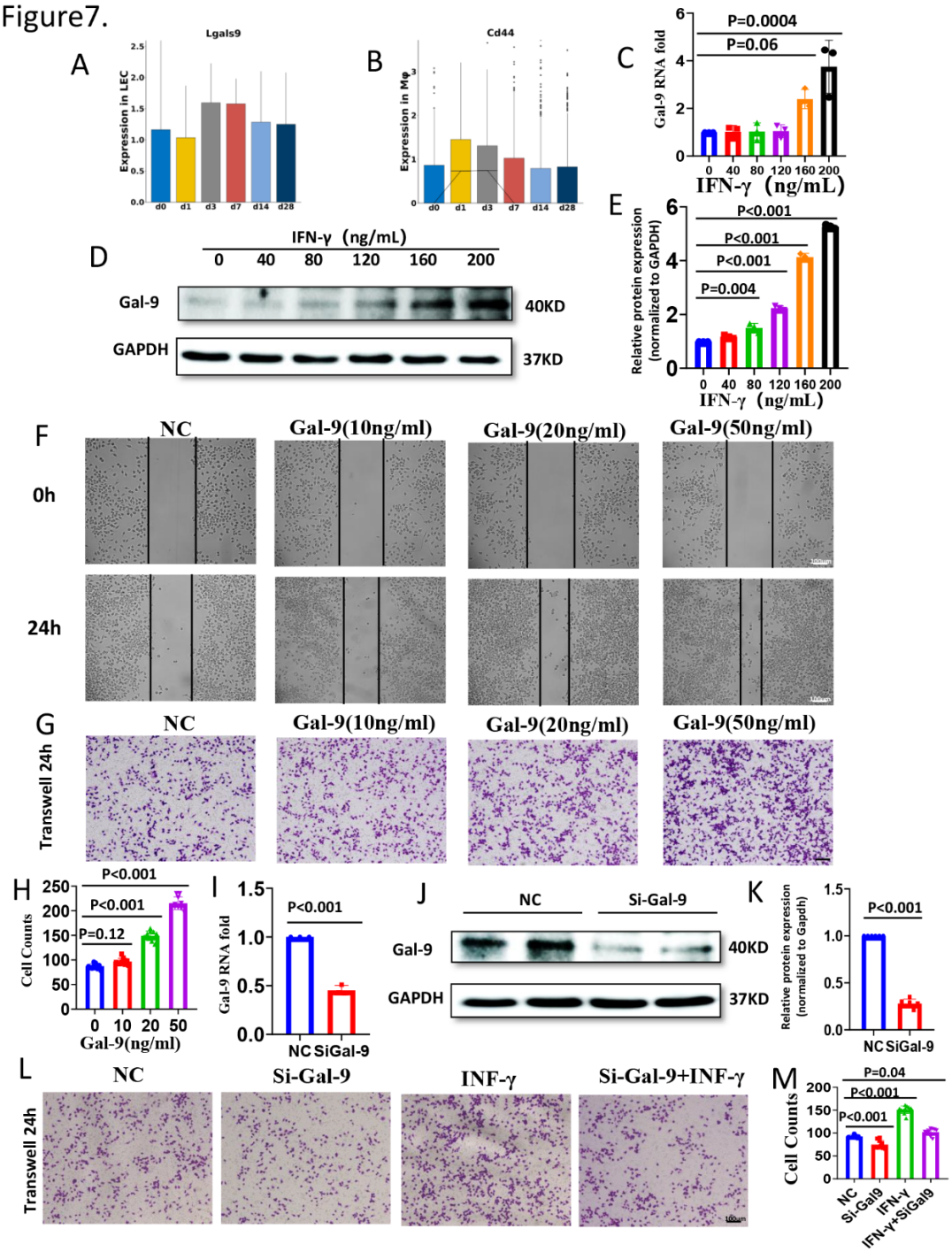

Figure 7. Possibility of LECs Affecting the Infiltration of Macrophages through the Galectin9-CD44 Pathway. (A and B) Expression of the gene Lgals9 and CD44 in LECs at each time point; **(C)** Gal-9 RNA expression in mLEC cell line under IFN-γ stimulation over different concentrations; **(D and E)** Gal-9 RNA expression in mLEC cell line under IFN-γ stimulation over different concentrations. **(F)** Mouse monocyte macrophage(J774A.1) wound healing assay under Gal-9 stimulation over different concentrations. **(G and H)** J774A.1 macrophage cultured in Transwell system under Gal-9 stimulation over different concentrations. **(I, J, and K)** Gal-9 RNA and protein expression after Lgals9 gene silenced. **(L and M)** J774A.1(in upper cabinet) and LEC (in lower cabinet) co-cultured in a transwell system under INF-γ stimulation with or without SiGal-9.

648 **Key Resources Table Template and Guidelines**

649

650 **Template:**

Key Resources Table				
Reagent type (species) or resource	**Designation**	**Source or reference**	**Identifiers**	**Additional information**
cell line (include species here)	Mouse lymphatic endothelial cell line	gifted by Prof. Lin Chen (Army Medical University, China).		
cell line (include species here)	Mouse monocyte macrophage(J774A.1)	FuHeng Cell Center(Shanghai, China)	FH0329	
transfected construct (include species here)	Transfection Reagent	PolyPlus, France	0000002157	
antibody	rabbit anti-Lyve1	Abcam	ab14917	IF：1:300
antibody	rabbit anti-Prox1	Abcam	ab199359	IF：1:300
antibody	mouse anti-Aqp1	Santa	sc-25287	IF：1:300 WB：1:1000
antibody	rabbit anti-Gal9	Abcam	ab69630	WB：1:1000

antibody	rabbit anti-GAPDH	CST	#5174	WB：1:1000
sequence-based reagent	Aqp1(F)	Sangon Biotech		ACCTGCTGGCGATTGACTACAC
sequence-based reagent	Aqp1(R)	Sangon Biotech		GTTTGAGAAGTTGCGGGTGAGC
sequence-based reagent	Lgals9(F)	Sangon Biotech		TCTACTCCTGGAATCCCTCCTGTG
sequence-based reagent	Lgals9(F)	Sangon Biotech		AACCTCGTAGCATCTGGCAAGAC
peptide, recombinant protein	Galectin-9/lGals9 protein	MedChemExpress	HY-P72637	
peptide, recombinant protein	Interferon-gama	MedChemExpress	HY-P73252	
chemical compound, drug	CoCl2	Sigma Aldrich	60818-250g	
software, algorithm	SPSS	Chicago, IL, USA		version 22.0

651